International Journal of Control
Publication details, including instructions for authors and subscription information:
http://www.informaworld.com/smpp/title~content=t713393989

Design framework for high-performance optimal sampled-data control with application to a wafer stage

Online Publication Date: 01 June 2007
To cite this Article: Oomen, T., van de Wal, M. and Bosgra, O. , (2007) 'Design framework for high-performance optimal sampled-data control with application to a wafer stage', International Journal of Control, 80:6, 919 - 934
To link to this article: DOI: 10.1080/00207170701216329
URL: http://dx.doi.org/10.1080/00207170701216329

International Journal of Control
Vol. 80, No. 6, June 2007, 919–934

Taylor & Francis
Taylor & Francis Group

Design framework for high-performance optimal sampled-data control with application to a wafer stage

T. OOMEN*†, M. VAN DE WAL‡ and O. BOSGRA†

†Mechanical Engineering, Control Systems Technology Group, Eindhoven University of Technology, P.O. Box 513, 5600 MB Eindhoven, The Netherlands
‡Philips Applied Technologies, Mechatronics Department, Drives & Control, HTC-7, 5656 AE Eindhoven, The Netherlands

(*Received 8 August 2006; in final form 12 January 2007*)

Control design for high-performance sampled-data systems with continuous time performance specifications is investigated. Direct optimal sampled-data control design explicitly addresses both the digital controller implementation and the intersample behaviour. The model that is required for direct optimal sampled-data control should evolve in continuous time. Accurate models for control design, however, generally evolve in discrete time since they are obtained by means of system identification techniques. The purpose of this paper is the development of a control design framework that enables the usage of models delivered by system identification techniques, while explicitly addressing both the digital controller implementation and the intersample behaviour aspects. Thereto, the incompatibility of the models delivered by system identification techniques and the models used in sampled-data control is analysed. To use models delivered by system identification techniques in conjunction with optimal sampled-data control, tools are employed that stem from multirate system theory. For the actual control design, key theoretical issues in sampled-data control, which include the linear periodically time-varying nature of sampled-data systems, are addressed. The control design approach is applied to the $\mathcal{H}_\infty$-optimal feedback control design of an industrial high-performance wafer scanner. Experimental results illustrate the necessity of addressing the intersample behaviour in high-performance control design.

List of abbreviations

CT	Continuous time
DT	Discrete time
DOF	Degree-of-freedom
IC	Integrated circuit
LPTV	Linear periodically time varying
LTI	Linear time invariant
MIMO	Multi-input multi-output
MR	Multirate
SD	Sampled-data
SISO	Single-input single-output
ZOH	Zero-order hold

*Corresponding author. Email: t.a.e.oomen@tue.nl

1. Introduction

Industrial high-precision six degrees-of-freedom (DOFs) positioning systems are subject to increasing demands regarding speed and accuracy. An example of such a system is a wafer stage that is part of a wafer scanner. These scanners are used for the production of integrated circuits (ICs); see Stix (1995). The market position of a wafer scanner is mainly determined by the accuracy of the produced ICs and by the throughput of the machine (Mack 2004). The accuracy translates into typical requirements of the wafer stage position accuracy in the order of nanometers, whereas the throughput translates into high scan velocities and accelerations of approximately $0.5\,\mathrm{m/s}$ and $10\,\mathrm{m/s^2}$, respectively. Besides a nearly perfect electromechanical design, a

International Journal of Control
ISSN 0020–7179 print/ISSN 1366–5820 online © 2007 Taylor & Francis
http://www.tandf.co.uk/journals
DOI: 10.1080/00207170701216329

state-of-the-art control system is indispensable for the satisfaction of these ever-increasing demands.

Optimal model-based control is a rigorous and systematic approach for designing high-performance controllers for multi-input multi-output (MIMO) systems. To achieve high performance, (i) the designed controller should be *implemented* accurately, (ii) the *model* should contain those aspects of the true system that are relevant for feedforward and feedback control design, and (iii) the performance and robustness requirements should be reflected in a suitably chosen *criterion*.

The performance of the controlled system is naturally evaluated in continuous time (CT). The controller, however, is *implemented* in a digital environment to enable high implementation flexibility and accuracy. The controlled system is thus a sampled-data (SD) system. In SD control design, three approaches can be distinguished:

(I) continuous time (CT) control design with a *posteriori* controller discretization;
(II) plant discretization and subsequent discrete time (DT) control design;
(III) direct SD control design.

In the first approach, the digital controller implementation is neglected during control design, whereas in the second approach intersample behaviour is ignored. Approaches I and II are standard in control design (Åström and Wittenmark 1990, Franklin *et al.* 1998) and result in satisfactory performance if the sampling frequency is well beyond the frequency of the dynamics to be controlled. In state-of-the-art motion control, however, the trend is that closed-loop bandwidth requirements increase due to increasing performance specifications, whereas the sampling frequency does not increase accordingly. In fact, the sampling frequency may even decrease due to the implementation of more complex control algorithms. Direct SD control design (Bamieh *et al.* 1991, Chen and Francis 1995) formally resolves these shortcomings of the classical approaches by explicitly addressing both the digital controller implementation and intersample behaviour issues.

The *model* that is used for control design should contain those aspects of the system that are relevant for closed-loop performance. In high-performance electromechanical motion systems, flexible dynamics limit the achievable performance of the controlled system and can even endanger closed-loop stability (Doyle and Stein 1981, Steinbuch and Norg 1998). System identification (SI) techniques are essential for the accurate and fast identification of these flexible dynamics. The experimental data that are used for SI are processed on a digital computer, hence the resulting model evolves in DT.

A standard assumption in direct SD control is that a CT model of the system is available. The discrepancy between the model that SI delivers and the model used in direct SD controller synthesis restricts the combination of the two in a control design procedure. Indeed, in previous applications of direct SD control to industrial systems (Kimura *et al.* 1996, Hirata *et al.* 2000), simplistic models were used that are not suitable for high-performance motion control design. The purpose of this paper is to develop a design framework that enables the usage of models from SI, while explicitly addressing both the digital controller implementation and the intersample behaviour aspects.

One approach to address the intersample behaviour without the need for a CT model is to consider the SD control problem as the limiting case of a multirate (MR) control problem (Chen and Francis 1995, Yamamoto *et al.* 1999). In an MR control problem (Kranc 1957, Vaidyanathan 1993) a DT plant is controlled by a DT controller that operates at a lower sampling frequency. The intersample behaviour is still addressed to a certain extent if a direct MR control problem is pursued, although the requirement of a CT model is avoided. Hence, the MR approach is an intermediate approach that falls between Approach II and Approach III, above.

Another design approach that is closely related to direct SD control design is digital controller redesign (Keller and Anderson 1992, Anderson 1993, Cantoni and Vinnicombe 2004). Digital redesign is a refinement of Approach I, above, where the open-loop approximation step is replaced by a closed-loop approximation involving an SD performance criterion. The requirement of a CT plant model can be relaxed by considering an MR digital redesign problem (Anderson 1993).

Independent of the control design approach pursued, the resulting controller is only useful if the control goal is accurately quantified by means of a suitable *criterion*. For linear time invariant (LTI) feedback systems, the control goal is often quantified in the frequency domain. The main motivation is that the frequency domain gives clear insight into the benefits and trade-offs that are present in control design. MR and SD systems, however, are linear periodically time varying (LPTV) (Chen and Francis 1995), and hence the notion of frequency response is not defined uniquely. The main reason for this non-uniqueness is the aliasing of signals in SD and MR systems. Alternative definitions of frequency response functions for SD systems include

- fundamental transfer function (FTF) (Goodwin and Salgado 1994, Freudenberg *et al.* 1995),
- performance frequency gain (PFG) (Cantoni and Glover 1997, Lindgärde and Lennartson 1997),

- robust frequency gain (RFG) (Araki *et al.* 1996, Yamamoto and Khargonekar 1996).

The FTF and PFG are most useful for performance quantification, but are not directly suitable for controller synthesis. Though the RFG is suitable for controller synthesis, it is more difficult to interpret. Thus, handling the LPTV aspects in the control design for MR and SD systems is not straightforward.

The contribution of this paper is the development of a design framework combining SI techniques with the advantages of direct SD control, i.e., the digital controller implementation and the intersample behaviour are both explicitly addressed. The key idea is to identify the plant at a higher sampling frequency than the frequency at which the resulting controller should operate. This is motivated by the fact that for real-time control the sampling time is lower bounded by the computational time required to determine a new controller input. This bound is not present for SI that can be performed off-line. The resulting control design problem is an MR problem, which resembles the direct optimal MR approach in Chen and Francis (1995). Whereas in Chen and Francis (1995) a direct MR approach is pursued to solve the direct SD optimal control problem, the present paper employs an MR approach for connecting SI with SD control and focuses on the LPTV aspects in MR control design. In the present approach, the difficulties with LPTV aspects in MR control are overcome by treating the digital controller implementation and intersample behaviour issues separately. In particular, the following points apply.

- The control design is performed in a standard LTI framework. An approach, which resorts to a Möbius transformation (Brown and Churchill 1996), for DT loopshaping using an $\mathcal{H}_\infty$ criterion is presented. Though the application of a Möbius transformation has been used before to solve the DT $\mathcal{H}_\infty$-optimal control problem (Iglesias and Glover 1991), the main contribution of the presented approach is the quantification of both the performance and robustness specifications in an auxiliary domain.
- Analysis of the resulting intersample behaviour is performed using new frequency domain MR analysis tools. The MR analysis tools are based on the developments in SD frequency response functions, i.e., the FTF, PFG, and RFG. Their definition and usage in an MR setting is new.
- Clear guidelines for the iterative improvement of the LTI control design are provided. The iterative design gives the control designer full control over the resulting closed-loop intersample behaviour without introducing any unnecessary approximations during the control design cycle. The explicit iterative approach to optimal SD control has not been attempted before in a frequency domain setting. In addition, the approach is experimentally demonstrated on an industrial wafer stage.

The paper is organized as follows. In § 2, optimal sampled-data control design is reviewed. Modelling for SD control is elaborated on and extensions to MR systems are presented in § 3. The quantification of the control goal is discussed in § 4, which leads to a control design procedure in § 5. In § 6, the proposed approach is demonstrated on a wafer stage. The experimental results illustrate the importance of intersample behaviour in an industrial application. Finally, conclusions are drawn in § 7.

2. Direct optimal SD control

In this section, the SD control design problem is defined. Also, the feasibility of the SD problem for electromechanical motion systems, such as wafer scanners, is evaluated.

Consider the setup of figure 1 (CT and DT signals are indicated by solid and dashed lines, respectively), where P_c is a CT plant model and K_d is a DT controller. Furthermore, $w \in \mathbb{R}^{n_w}$ denotes the weighted exogenous signals that enter the control system, e.g., reference signals and disturbances, and $z \in \mathbb{R}^{n_z}$ denotes the weighted exogenous outputs, e.g., tracking errors and actuator inputs that are defined such that they are ideally zero. Fictitious exogenous inputs and outputs can be incorporated to represent model uncertainty. The standard plant G_c is defined as

$$G_c = W\mathcal{F}_u(J, P_c)V, \tag{1}$$

where W and V are appropriate weighting filters, J is an interconnection matrix having only -1, 0, or 1 entries, and $\mathcal{F}_u$ is the upper linear fractional transformation

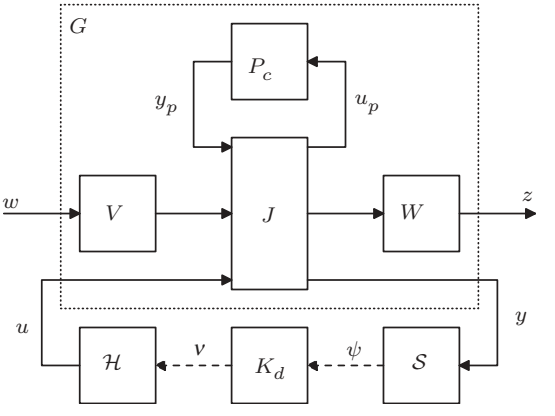

Figure 1. SD standard plant.

(LFT) (Zhou *et al.* 1996). Sampled measurements $\psi \in \mathbb{R}^{n_y}$ are provided by the ideal sampler $\mathcal{S}$ from the measured signal $y \in \mathbb{R}^{n_y}$. Quantization effects (Bamieh 2003) are not addressed since the discrete time signals are assumed to take values in $\mathbb{R}$. The control signal $u \in \mathbb{R}^{n_u}$ that is applied to the plant is reconstructed from the discrete time control signal $v \in \mathbb{R}^{n_u}$ by a zero-order-hold (ZOH) reconstructor $\mathcal{H}$. Furthermore, it is assumed that $\mathcal{S}$ and $\mathcal{H}$ are synchronized and operate equidistantly in time with fixed period $h = (2\pi/\omega_s) \in \mathbb{R}_+$, where ω_s is the sampling frequency in (rad/s).

The SD controller synthesis problem (Chen and Francis 1995) is defined as follows.

Definition 1: Given the SD standard plant in figure 1, containing a CT plant model, appropriate weighting filters, and a prespecified sampling frequency ω_s, the SD controller synthesis problem amounts to computing

$$K_d = \arg \min_{\text{stabilizing } K_d} \|\mathcal{F}_l(G_c, \mathcal{H}K_d\mathcal{S})\|, \tag{2}$$

where $\|\cdot\|$ denotes a suitable norm and $\mathcal{F}_l$ denotes the lower LFT.

The first question that arises is whether there exists a stabilizing controller in the SD problem of Definition 1, since stabilizability and detectability can be lost by sampling. From a control perspective, the plant is fixed and the weighting filters W and V can be chosen freely. Therefore, restrictions on admissible sampling frequencies, for which a stabilizing controller exists, are only imposed by the plant. Let P_c be LTI and represented by the state-space model

$$P_c = \left[\begin{array}{c|c} A_c^p & B_c^p \\ \hline C_c^p & D_c^p \end{array}\right] := C_c^p(sI - A_c^p)^{-1}B_c^p + D_c^p, \tag{3}$$

where $A_c^p \in \mathbb{R}^{n_x \times n_x}$, $B_c^p \in \mathbb{R}^{n_x \times n_u}$, $C_c^p \in \mathbb{R}^{n_y \times n_x}$, $D_c^p \in \mathbb{R}^{n_y \times n_u}$ and the complex indeterminate s is the Laplace variable in case of continuous time systems. Let the ith eigenvalue $\lambda_i^p(A_c^p)$ of A_c^p be given by

$$\lambda_i^p(A_c^p) = \sigma_i^p + j\omega_i^p, \quad i = 1, \ldots, n_x. \tag{4}$$

Definition 2: If A_c^p has two eigenvalues λ_i^p, λ_j^p, $i \neq j$ that satisfy

$$\left\{\lambda_i^p, \lambda_j^p | \sigma_i^p = \sigma_j^p \quad \text{and} \quad \omega_i^p = \omega_j^p + l\omega_s, l \in \mathbb{Z}\backslash\{0\}\right\}, \tag{5}$$

then the sampling frequency ω_s is pathological with respect to A_c^p. If A_c^p does not have two eigenvalues that satisfy (5), then the sampling frequency is non-pathological.

The notion of pathological sampling enables the derivation of the following well-known result.

Theorem 1: *Consider the system* (3) *and let the sampling frequency be non-pathological with respect to* A_c^p *for all* λ_i^p *satisfying* $\sigma_i^p \geq 0$. *Then, there exists a DT controller* K_d *that stabilizes* P_c.

For a proof of Theorem 1; see Kalman *et al.* 1963 or Chen and Francis 1995. The implications of Theorem 1 are investigated for electromechanical motion systems. Electromechanical motion systems are mechanical structures that are electrically actuated and the output is a position or a derivative thereof. Generally, such systems have n_{rb} rigid-body modes, corresponding to the motion DOFs. In addition to the rigid-body dynamics, parasitic dynamics are present in any realistic system, e.g., due to mechanical flexibilities, actuator dynamics, or sensor dynamics.

Assumption 1: *The true electromechanical system* P_t *evolves in CT and is assumed to be LTI. Moreover, it has a state-space realization*

$$P_t = \left[\begin{array}{cc|c} A_{rb} & 0 & B_{rb} \\ 0 & A_f & B_f \\ \hline C_{rb} & C_f & 0 \end{array}\right], \tag{6}$$

where $A_{rb} \in \mathbb{R}^{2n_{rb} \times 2n_{rb}}$ *corresponds to the rigid-body dynamics and satisfies* $\lambda_i(A_{rb}) = 0$, $i = 1, \ldots, 2n_{rb}$, (A_{rb}, B_{rb}) *controllable, and* (A_{rb}, C_{rb}) *observable. Furthermore,* A_f *satisfies* $\mathrm{Re}(\lambda_i(A_f)) < 0$.

The particular structure for motion systems of Assumption 1 ensures the existence of a stabilizing controller K_d for a given sampling frequency ω_s.

Lemma 1: *Consider the system of Assumption* 1. *Then there exists a controller that stabilizes the SD system of figure* 1 *for all* $\omega_s \in \mathbb{R}$, $\omega_s > 0$.

Proof: The system matrix of P_t in (6) has $2n_{rb}$ controllable and observable eigenvalues $\lambda(A_{rb})$ satisfying $\mathrm{Re}(\lambda_i) \geq 0$, $i = 1, \ldots, 2n_{rb}$ and the remaining eigenvalues $\lambda(A_f)$ satisfying $\mathrm{Re}(\lambda_i) < 0$, $i = 2n_{rb} +, \ldots, \infty$. By Theorem 1, to verify the existence of a stabilizing K_d for P_t, it is sufficient to evaluate the pathological sampling condition with respect to A_{rb}. Since $\lambda_i(A_{rb}) = 0$, $i = 1, \ldots, 2n_{rb}$, the sampling frequency is non-pathological with respect to A_{rb}, and hence there exists a stabilizing K_d for all $\omega_s > 0$. □

Remark 1: In some cases, Assumption 1 may not be fulfilled, i.e., the plant system matrix may contain a finite number of eigenvalues in the closed right half plane in addition to the $2n_{rb}$ eigenvalues at zero. Let $\bar{\omega}_r$ denote the maximum absolute imaginary part of the unstable eigenvalues. Then, to achieve good performance and robustness properties of the resulting sampled-data control system, choose $\omega_s > \bar{\omega}_r$.

Furthermore, there exists a stabilizing controller for the unstable plant for all $\omega_s > \bar{\omega}_r$.

The SD control problem of Definition 1 is a meaningful problem for the class of systems in Assumption 1, since the true system and all exogenous signals evolve in CT. Thus, intersample behaviour is fully addressed in (2). Furthermore, all aspects involved in the digital controller implementation, such as the aliasing of signals, are automatically handled by the SD control problem. In virtue of Lemma 1, a solution to the SD problem of Definition 1 exists for the system (6) and a given arbitrary sampling frequency ω_s.

Solutions for the computation of a controller that minimizes an SD system norm are available in the lifting framework (Bamieh *et al.* 1991). Particular usage of the lifting framework in the SD $\mathcal{H}_2$-optimal control problem are given in Bamieh and Pearson 1992a and Chen and Francis 1995. For SD $\mathcal{H}_\infty$-optimal solutions, see, e.g., Bamieh and Pearson 1992b and Chen and Francis 1995. The SD ℓ_1-optimal solution is treated in Bamieh *et al.* 1993. Furthermore, SD controller synthesis algorithms are available in commercial software packages (Balas *et al.* 2001).

The remaining issues are the modelling of the plant P_c and the selection of the weighting filters W and V. Firstly, the modelling issue is elaborated on in § 3, since the choice of weighting filters depends on the properties of the plant.

3. Modelling for SD control design

Standard SD controller synthesis algorithms require a finite dimensional (FD) LTI model P_c of the true system. No true physical system can be described exactly by a model, hence there is always a discrepancy between the model and the true system. Robust control enables the explicit incorporation of an uncertainty model into the control design procedure. In this section, the modelling of a nominal plant model is considered. Uncertainty modelling is briefly addressed in §§ 4 and 5.

As mentioned earlier, SI techniques are indispensable for the accurate modelling of electromechanical systems for control design. SI should be performed in closed-loop since the open-loop system (6) is unstable. Then, the data used for SI are typically extracted from the DT control loop, e.g., the plant input v_p, plant output ψ_p, and external reference ρ, see figure 2. The model used in SD control design, however, evolves in CT time, i.e., it represents the relation between u_p and y_p in figure 2. This leads to the following identification problem.

Problem 1: Given sampled measurements of the system, the SI for SD control problem amounts to determining P_c, which is a CT model that is accurate for SD control design.

Problem 1 can be decomposed into two subproblems. First, identify a DT model P_d using standard SI techniques, see, e.g., Ljung 1999. Next, compute P_c from the relation

$$P_d = \mathcal{S} P_c \mathcal{H}. \tag{7}$$

P_d is called the ZOH discretization of P_c, with a state-space realization given by

$$P_d = \left[\begin{array}{c|c} A_p^d & B_p^d \\ \hline C_d^p & D_p^d \end{array}\right], \tag{8}$$

where the dimensions are equal to (3). A necessary condition for reconstructing P_c uniquely from P_d is that the eigenvalues $\lambda_i(A_c^p)$ can be reconstructed from $\lambda_i(A_d^p)$, $i = 1, \ldots, n_x$. The mapping of these eigenvalues is given by

$$\lambda_i\left(A_d^p\right) = e^{\lambda_i(A_c^p)h} = e^{\sigma_i h} e^{j\omega i h}, \tag{9}$$

which is definitely not an injection since it is periodic with period $(2\pi/h)$. Hence, a sufficient condition for the unique computation of $\lambda_i(A_c^p)$ is

$$|\omega_i| < \frac{\pi}{h}, \quad i = 1, \ldots, n_x. \tag{10}$$

Condition (10) is not satisfied in general since the location of the eigenvalues of the underlying CT plant is not known *a priori*. Another complication in the computation of P_c from P_d, see (7), is the mapping of plant zeros that is significantly more involved than the mapping of plant poles (Åström *et al.* 1984). Thus, the modelling of a CT model from DT data is not straightforward and in general does not result in a unique model. It is impossible to decide whether a particular model P_c satisfying (7) is suitable for SD control design based on sampled measurements of the true system, because each of the CT models satisfying (7) has an identical response at the sampling instants.

The sampling frequency of the DT model is determined by the sampling frequency ω_s of the data used for SI. The sampling frequency of the controller is mainly limited by the computational time required to compute a new controller input in between two sampling instants. SI, however, can be performed off-line and is thus

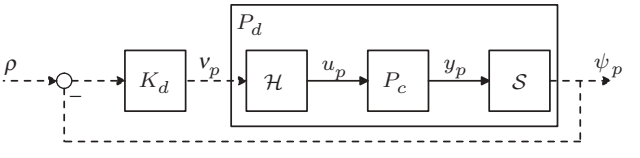

Figure 2. SI for SD control.

computationally less expensive than high performance control. Hence, it is often possible to extract data at a higher sampling frequency than the frequency at which the resulting high-performance controller is operating at, e.g., by

- implementing a low-complexity controller that requires less computational time and thus can be implemented with a higher sampling frequency, or
- using dedicated data acquisition equipment.

The resulting DT model operates at a higher sampling frequency $\omega_{s,h} > \omega_s$ and thus represents more intersample information of the underlying CT system than the model P_d.

In the remainder of this section tools are presented that enable the construction of a MR standard plant that resembles the SD standard plant, see figure 1. The following assumption ensures that the plant model, operating at the relatively high sampling frequency $\omega_{s,h}$, can be interconnected with a controller, operating at a lower sampling frequency ω_s, using standard tools from MR signal processing (Vaidyanathan 1993).

Assumption 2: *Let the sampling frequencies $\omega_{s,h}$ and ω_s be related by*

$$\omega_{s,h} = F\omega_s, \quad F = 2, 3, \ldots. \tag{11}$$

The following definitions represent MR equivalents to the SD sampler and reconstructor. Let the DT signals v_h and v be defined as

$$v_h[k] := u(kh_h) \tag{12}$$

$$v[k] := u(kh) = u(kFh_h), \tag{13}$$

where $h_h := (2\pi/\omega_{s,h})$.

Definition 3 (Vaidyanathan 1993)**:** The downsampling operation is defined by

$$v[k] = \mathcal{S}_d(v_h[k]) := v_h[Fk]. \tag{14}$$

The Fourier transforms $N(e^{j\omega h})$ and $N_h(e^{j\omega h_h})$ of v and v_h, respectively, are related by

$$N(e^{j\omega h}) = \frac{1}{F}\sum_{f=0}^{F-1} N_h\left(e^{jh_h(\omega-(f/F)\omega_{s,h})}\right). \tag{15}$$

Definition 4 (Vaidyanathan 1993)**:** The upsampler is defined by

$$v_h[k] = \mathcal{S}_u(v[k]) := \begin{cases} v\left[\dfrac{k}{F}\right] & \text{for } \dfrac{k}{F} \in \mathbb{Z} \\ 0 & \text{for } \dfrac{k}{F} \notin \mathbb{Z}. \end{cases} \tag{16}$$

The Fourier transforms are related by

$$N_h(e^{j\omega h_h}) = N(e^{j\omega h}). \tag{17}$$

The upsampler inserts zeros in between the values of the slowly sampled signal v. These values have to be interpolated in order to obtain the MR equivalent of the SD ZOH reconstructor as shown in figure 1.

Definition 5: The ZOH interpolator is defined as

$$\mathcal{I}_{ZOH}(z) = \sum_{f=0}^{F-1} z^{-f}, \tag{18}$$

where z is a complex indeterminate.

Definition 6: The MR ZOH reconstructor is defined as

$$\mathcal{H}_u := \mathcal{I}_{ZOH}(z)S_u. \tag{19}$$

If the sampling frequency $\omega_{s,h}$ is chosen as the maximal value that the data acquisition hardware allows, then the model $P_{d,h}$, operating at the sampling frequency $\omega_{s,h}$, contains as much intersample information as can be obtained by equidistant sampling from the underlying CT system P_c. Furthermore, the model sampled with sampling frequency $\omega_{s,h}$ can be downsampled to the model operating at a low sampling frequency ω_s, see also figure 2.

Lemma 2: *Let a model of the system with sampling frequency $\omega_{s,h}$ be given by*

$$P_{d,h} = \left[\begin{array}{c|c} A^p_{d,h} & B^p_{d,h} \\ \hline C^p_{d,h} & D^p_{d,h} \end{array}\right]. \tag{20}$$

A state-space realization of the downsampled system, see figure 2 and (8)*, is given by*

$$\begin{bmatrix} A^p_d & B^p_d \\ \star & \star \end{bmatrix} = \begin{bmatrix} A^p_{d,h} & B^p_{d,h} \\ 0 & I \end{bmatrix}^F \tag{21}$$

$$C^p_d = C^p_{d,h} \tag{22}$$

$$D^p_d = D^p_{d,h}, \tag{23}$$

where $\star$ denotes an irrelevant matrix entry and F is defined in (11)*.*

Proof: Equations (21)–(23) follow directly from successive substitution of the state equation $\xi_h[k+1] = A^p_{d,h}\xi_h[k] + B^p_{d,h}v_h[k]$ and using $v_h[k+f] = v[k/F]$, $f = 0, \ldots, F-1$. □

From Lemma 2, it directly follows that $A^p_{d,h}$ cannot be reconstructed uniquely from A^p_d due to the relation $A^p_d = (A^p_{d,h})^F$. By replacing the CT model of figure 1 with

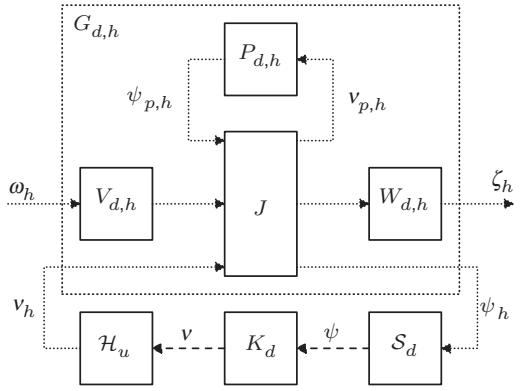

Figure 3. MR standard plant.

the fast sampled model $P_{d,h}$, an MR standard plant is obtained, see figure 3, where

$$G_{d,h} = W_{d,h}\mathcal{F}_u(J, P_{d,h})V_{d,h}. \tag{24}$$

This MR standard plant represents all intersample behaviour that can be obtained from experimental modelling. Hence the MR standard plant is the best approximation of the SD standard plant in the sense of modelling limitations. This leads to the following definition of the MR controller synthesis problem:

Definition 7: Given the MR standard plant in figure 3, containing a DT plant model $P_{d,h}$ and appropriate weighting filters with sampling frequency $\omega_{s,h}$, the MR controller synthesis problem amounts to computing

$$K_d = \arg \min_{\text{stabilizing } K_d} \|\mathcal{F}_l(G_{d,h}, \mathcal{H}_u K_d \mathcal{S}_d)\|, \tag{25}$$

where $\|\cdot\|$ denotes a suitable norm.

Standard system identification techniques can be applied to obtain a unique model $P_{d,h}$. Hence, only the weighting filters $W_{d,h}$ and $V_{d,h}$ need to be defined to quantify the performance and robustness specifications in (25) and (24). This is elaborated on in the next section.

4. Control goal quantification

The MR controller synthesis problem of Definition 7 is the best feasible approximation of the SD control problem in terms of modelling limitations. The performance and robustness requirements of the control system should be reflected in a suitably chosen criterion, see (25). An $\mathcal{H}_\infty$-norm is particularly useful since it resembles well-known classical loopshaping techniques and enables the explicit incorporation of model uncertainty into the control design procedure. In particular, the weighting filters $V_{d,h}$ and $W_{d,h}$ for control goal quantification can be signal-based or loopshaping-based (Skogestad and Postlethwaite 2005). A signal-based approach amounts to quantifying the estimated and desired spectral contents of exogenous inputs and outputs, respectively. Accurately identifying the disturbances in a realistic system, however, is generally too time consuming. Hence, in practice a signal-based approach to weighting filter selection is often avoided.

Often, the performance weights in $\mathcal{H}_\infty$-optimal control are based on loopshaping techniques. Loopshaping design amounts to shaping either open-loop (McFarlane and Glover 1992) or closed-loop (van de Wal *et al.* 2002) transfer functions. In many cases, a clear idea is available regarding the desired loopshape. The loopshaping procedure is based on the fact that sinusoids are eigenfunctions of LTI systems, such as CT or DT systems. The MR system of figure 3, however, is LPTV with period $F=(h/h_h)$, see Bamieh *et al.* 1991. A frequency domain analysis of the system of figure 3 is performed. The development is to a large extent analogous to the SD frequency response functions; see Goodwin and Salgado (1994), Freudenberg *et al.* (1995), Araki *et al.* (1996), Yamamoto and Khargonekar (1996), Lindgärde and Lennartson (1997), and Cantoni and Glover (1997).

Lemma 3: *Let $\omega_h[k]$ be a signal with DT Fourier transform $\Omega_h(e^{j\omega h_h})$ that is applied to the MR system of figure* 3. *Then the DT Fourier transform of the output $\zeta_h[k]$ is given by*

$$\begin{aligned} Z_h(e^{j\omega h_h}) &= G_{11d,h}\big(e^{j\omega h_h}\big)\Omega_h\big(e^{j\omega h_h}\big) \\ &\quad + G_{12d,h}\big(e^{j\omega h_h}\big)\mathcal{I}_{ZOH}(e^{j\omega h_h})Q_d\big(e^{j\omega h}\big) \\ &\quad \cdot \frac{1}{F}\sum_{f=0}^{F-1} G_{21d,h}\big(e^{jh_h(\omega-(f/F)\omega_{s,h})}\big)\Omega_h\big(e^{jh_h(\omega-(f/F)\omega_{s,h})}\big), \end{aligned} \tag{26}$$

where

$$Q_d\big(e^{j\omega h}\big) = \big(I - K_d\big(e^{j\omega h}\big)G_{22d}\big(e^{j\omega h}\big)\big)^{-1}K_d\big(e^{j\omega h}\big) \tag{27}$$

and G_{22d} denotes the downsampled $G_{22d,h}$, see Lemma 2, *with appropriate partitioning of $G_{d,h}$, i.e.*,

$$G_{d,h} = \begin{pmatrix} G_{11d,h} & G_{12d,h} \\ G_{21d,h} & G_{22d,h} \end{pmatrix}. \tag{28}$$

The proof results from extensive but straightforward manipulations using (15), (17), and (18). Equation (26) reveals the LPTV nature of the MR system of figure 3 since the frequency separation principle does not hold. By selecting the fundamental component, i.e., $f=0$, the MR equivalent of the FTF, denoted as $\mathcal{F}(e^{j\omega h_h})$, is obtained.

Definition 8: The function $\mathcal{F}(e^{j\omega h_h})$ for the system of figure 3 is defined as

$$\mathcal{F}\left(e^{j\omega h_h}\right) = G_{11d,h}\left(e^{j\omega h_h}\right) + \frac{1}{F} G_{12d,h}\left(e^{j\omega h_h}\right) \cdot \mathcal{I}_{ZOH}\left(e^{j\omega h_h}\right) Q_d\left(e^{j\omega h}\right) G_{21d,h}\left(e^{j\omega h_h}\right). \quad (29)$$

$\mathcal{F}$ does not represent the full intersample behaviour since the aliasing components $f \neq 0$ in (26) are neglected. To evaluate the full intersample behaviour, define the signal spaces

$$\mathcal{W}_D = \left\{\omega_h[k] \omega_h[k] = c e^{j\omega k h_h}, \|c\|_2 < \infty\right\} \quad (30)$$

$$\mathcal{W}_{MR} = \left\{\omega_h[k] | \omega_h[k] = \sum_{l=0}^{F-1} c_l e^{jkh_h(\omega - f\omega_s)}, \|c_l\|_2 < \infty\right\}. \quad (31)$$

Definition 9: Let $\omega_h[k] \in \mathcal{W}_D$ be applied to the MR system of figure 3. Then $\mathcal{P}(e^{j\omega h_h})$ is defined as

$$\mathcal{P}\left(e^{j\omega h_h}\right) = \sup_{\omega_h \neq 0} \frac{\|\zeta_h\|_{\mathcal{P}}}{\|\omega_h\|_{\mathcal{P}}}, \quad (32)$$

where

$$\|\cdot\|_{\mathcal{P}} = \sqrt{\lim_{N\to\infty} \frac{1}{2N+1} \sum_{k=-N}^{N} \|\cdot\|^2} \quad (33)$$

and $\|\cdot\|$ denotes the Euclidean vector norm.

Lemma 4: *$\mathcal{P}(e^{j\omega h_h})$, i.e., $\mathcal{P}$ evaluated at frequency ω_0, is given by*

$$\mathcal{P}\left(e^{j\omega h_h}\right) = \sqrt{\bar{\lambda}(A(\omega_0))}, \quad (34)$$

where the matrix $A(\omega_0)$ is defined as

$$A(\omega_0) = \sum_{f=0}^{F-1} \left\| c_f(\omega_0) \right\|^2 \quad (35)$$

and

$$c_f(\omega_0) = \begin{cases} G_{11d,h}\left(e^{j\omega_0 h_h}\right) + \frac{1}{F} G_{12d,h}\left(e^{j\omega_0 h_h}\right) \mathcal{I}_{ZOH}\left(e^{j\omega_0 h_h}\right) \\ \quad Q_d\left(e^{j\omega_0 h}\right) G_{21d,h}\left(e^{j\omega_0 h_h}\right), & f = 0 \\ \frac{1}{F} G_{12d,h}\left(e^{jh_h(\omega_0 + (f/F)\omega_{s,h})}\right) \mathcal{I}_{ZOH}\left(e^{jh_h(\omega_0 + (f/F)\omega_{s,h})}\right) \\ \quad Q_d\left(e^{j\omega_0 h}\right) G_{21d,h}\left(e^{j\omega_0 h_h}\right), & f \neq 0 \end{cases} \quad (36)$$

The proof of Lemma 4 proceeds along similar lines as the SD PFG, see Lindgärde and Lennartson 1997, with the key difference that for the MR case no infinite summations are required. $\mathcal{P}$ represents the full intersample response to sinusoidal input signals in the sense of the power norm and can be computed using Lemma 4. However, sinusoidal signals of a single frequency are not eigenfunctions of the system presented in figure 3. Another definition for the frequency response of MR systems arises from the observation that the signal space $\mathcal{W}_{MR}$ is invariant under filtering by the MR system that is depicted in figure 3.

Definition 10: Let $\omega_h[k] \in \mathcal{W}_{MR}$ be applied to the MR system of figure 3. Then $\mathcal{R}(e^{j\omega h_h})$ is defined as

$$\mathcal{R}\left(e^{j\omega h_h}\right) = \sup_{\omega_h \neq 0} \frac{\|\zeta_h\|_2}{\|\omega_h\|_2}. \quad (37)$$

From Definition 10 it is clear that $\mathcal{R}$ is periodic with ω_s. The computation of $\mathcal{R}$ has been addressed in Yamamoto *et al.* 1999, where it is used to compute the RFG for SD systems. The peak value over frequency of $\mathcal{R}$ equals the $\mathcal{H}_\infty$-norm of the MR system, i.e.,

$$\|\mathcal{F}_l(G_{d,h}, \mathcal{H}_u K_d \mathcal{S}_d)\|_\infty = \sup_{\omega \in [0, \omega_s)} \mathcal{R}\left(e^{j\omega h_h}\right). \quad (38)$$

For performance analysis, it is useful to study the system response to single frequency sinusoidal input signals. Hence, the $\mathcal{F}$ and $\mathcal{P}$ are useful for frequency domain performance evaluation of MR systems. However, there is no one-to-one relation between an SD system norm and the functions $\mathcal{F}$ and $\mathcal{P}$, which limits their applicability for performance quantification. Though the function $\mathcal{R}$ has a one-to-one relation with the MR $\mathcal{H}_\infty$-optimal system norm, see (38), the function $\mathcal{R}$ is not suitable for performance analysis and loopshaping-based performance quantification since it is desirable to distinguish input frequencies separated by ω_s and not to collect them, see (31). The assertion that it is undesirable to collect input frequencies separated by ω_s is justified in § 6.

Besides the quantification of the performance goals, it is desirable to quantify model uncertainty such that robust performance can be guaranteed. The small-gain theorem (Zhou *et al.* 1996) provides a condition for closed-loop stability robustness analysis. To illustrate the usage of model uncertainty in robustness analysis for MR systems, consider the MR system depicted in figure 3. Let ω_h and ζ_h be fictitious exogenous inputs and outputs to represent model uncertainty, i.e., $\omega_h = \Delta \zeta_h$, where Δ is a bounded operator mapping ℓ_2 to ℓ_2. Then the closed-loop system is stable if and only if

$$\|\Delta \mathcal{F}_l(G_{d,h}, \mathcal{H}_u K_d \mathcal{S}_u)\|_\infty < 1. \quad (39)$$

If Δ is an LPTV operator, a necessary and sufficient condition for robust stability is that (Chen and Francis 1995)

$$\|\Delta\|_\infty \|\mathcal{F}_l(G_{d,h}, \mathcal{H}_u K_d \mathcal{S}_u)\|_\infty < 1. \quad (40)$$

If Δ is scaled, i.e., $||\Delta||_\infty \leq 1$, then robust stability is achieved if $\|\mathcal{F}_l(G_{d,h}, \mathcal{H}_u K_d \mathcal{S}_u)\|_\infty < 1$. Equation (38)

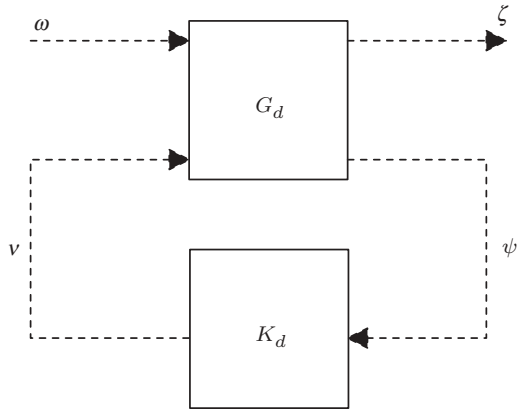

Figure 4. DT standard plant.

now implies that $\mathcal{R}$ can be used for robust stability analysis with respect to LPTV uncertainty. However, in practice it is more natural to study robust stability with respect to LTI perturbations since the CT plant P_c is assumed to be LTI. Then, (40) is a sufficient condition for robust stability and as such introduces conservatism.

If the plant model is downsampled using Lemma 2 before constructing a standard plant, i.e., if all intersample behaviour information is discarded, the DT standard plant as depicted in figure 4 is obtained. The system of figure 4 is LTI, hence sampled sinusoids of a single frequency are eigenfunctions of the system. This implies that Definitions 8, 9 and 10 coincide. In this case, $\mathcal{D}$ is obtained.

Definition 11 (Skogestad and Postlethwaite 2005)**:** Consider the system of figure 4. Then $\mathcal{D}(e^{j\omega h})$ is defined as

$$\mathcal{D}(e^{j\omega h}) = \bar{\sigma}(\mathcal{F}_l(G_d, K_d)). \tag{41}$$

Remark 2: The functions $\mathcal{D}$, $\mathcal{F}$, $\mathcal{P}$ and $\mathcal{R}$ can be evaluated for each entry of the vector valued signals ω_h and ζ_h individually to obtain an $n_z \times n_w$ frequency dependent matrix, or all at once to obtain a scalar frequency dependent function. The former is especially useful for performance analysis.

The fact that the downsampled system is LTI significantly simplifies the control design both with respect to performance and to robustness specifications. This fact is exploited in the next section, where the control design procedure is presented.

5. Control design procedure

A design framework is presented where the digital controller implementation and the intersample behaviour issues are both explicitly addressed. The setup depicted in figure 3 is used, which represents the best feasible approximation of the SD control problem in the sense of modelling limitations. The key issue is that the design aspect, i.e., how to quantify performance and robustness specifications, is not straightforward in an MR setting. The main reason is that the notion of frequency response is not defined uniquely; see § 4.

If the resulting controller should achieve high-performance, the performance specifications have be accurately quantified and design trade-offs should be carefully addressed. Furthermore, to avoid overly conservative control designs, the set of candidate plants that is introduced by the uncertainty model should not be too large. To satisfy these demands, the digital controller implementation and intersample behaviour issues are addressed separately during the control design procedure. First, the digital implementation is discussed in § 5.1. Next, the intersample behaviour is discussed in § 5.2. The design procedure involves six steps and is mainly focused on the feedback control design.

5.1 *Addressing digital controller implementation*

The first part of the control design procedure amounts to the design of a controller based on a DT plant model with the same sampling frequency ω_s as the controller that is to be designed, see figure 4. The setup of figure 4 is obtained from the MR setup of figure 3 by application of Lemma 2. The main motivation is that an LTI control structure is obtained. This enables a straightforward interpretation of performance measures, e.g., using Bode diagrams of closed-loop transfer functions, and robustness measures, e.g., gain margins, phase margins, and robustness to LTI model perturbations. Also, performance limitations such as the Bode sensitivity integral (Sung and Hara 1988) can easily be interpreted. Though the Bode sensitivity integral also exists for LPTV systems (Sandberg and Bernhardsson 2005), it is hard to interpret since for performance analysis it is useful to study the closed-loop system response with respect to sinusoidal signals of a single frequency and not signals in the class (31). Note that the stabilization aspect of the control design procedure is completely addressed. In particular, if K_d stabilizes P_d then it also stabilizes $P_{d,h}$ and the underlying CT plant P_c under the same assumptions as in Lemma 1.

The Tustin transformation, which is a special case of the Möbius transformation (Brown and Churchill 1996), is employed to facilitate the design procedure since it

enables the design of DT controllers using CT intuition. The Tustin transformation is defined as

$$w = \frac{2(z-1)}{h(z+1)}, \quad z = \frac{hw+2}{hw-2}. \tag{42}$$

The motivation for using the transformation (42) is twofold. Firstly, loopshaping-based weighting filters are often defined in terms of cut-off frequencies and asymptotes (van de Wal *et al.* 2002). Asymptotic behaviour of frequency response functions is based on the Bode gain-phase relation (Bode 1945). The Bode gain-phase relation only holds for CT systems, and thus not for $P_d(z)$. By transforming $P_d(z)$ to the auxiliary w-domain using (42), a system $P_d(w)$ with CT properties is obtained. The frequency response is then obtained by substituting $w = j\nu$ and satisfies

$$P_d(w)|_{w=j\nu} = P_d(z)|_{z=e^{j\omega h}}, \tag{43}$$

where the frequency axis is rescaled by

$$\nu = \frac{2}{h}\tan\left(\frac{\omega h}{2}\right). \tag{44}$$

Now the loopshaping design approach can be applied in the w-domain with fictitious frequency ν since the frequency response is preserved and the Bode gain-phase relation applies; see also Oomen *et al.* (2006). Secondly, the $\mathcal{H}_\infty$-norm is invariant under the transformation (42). Hence, readily available CT algorithms can be used; see, e.g., Balas *et al.* (2001) for $\mathcal{H}_\infty$-optimization and Wortelboer (1993) for model reduction tools.

Step 1: Define the control goal and control structure. This amounts to selecting the signals ω_h, ζ_h, ψ, and ν in figure 3. By downsampling, the setup of figure 4 is obtained. For feedback control design it makes sense to select the signals ω, ζ, ν, and ψ, as depicted in figure 5, where $\zeta = [\zeta_1^T \ \zeta_2^T]^T$ and $\omega = [\omega_1^T \ \omega_2^T]^T$; see also van de Wal *et al.* (2002). The weighted closed-loop transfer function matrix (TFM) M_d, determined by $\zeta = M_d\omega$, is given by

$$M_d = -\begin{bmatrix} W_{d,1}S_dV_{d,1} & W_{d,1}S_dP_dV_{d,2} \\ W_{d,2}K_dS_dV_{d,1} & W_{d,2}K_dS_dP_dV_{d,2} \end{bmatrix}, \tag{45}$$

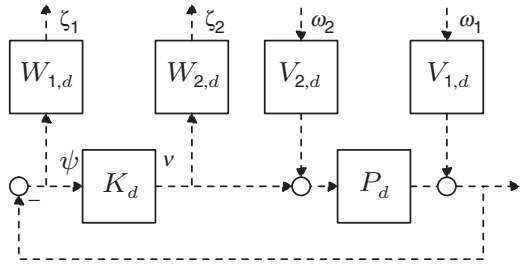

Figure 5. Four-block problem used for feedback control design.

where

$$S_d = (I + P_dK_d)^{-1}. \tag{46}$$

The TFM (45) contains all relevant closed-loop transfer functions and is a sensible control problem, see, e.g., Englehart and Smith 1991. A similar four-block problem arises in the open-loop loopshaping procedure in McFarlane and Glover 1992. In the remainder of this section, it is assumed that

- $\dim(\psi) = \dim(\nu)$, i.e., P_d is square,
- ν and ψ are selected such that P_d is decoupled at low frequencies,
- the plant rolls-off at high frequencies.

Step 2: Identify the plant at the maximal frequency $\omega_{s,h}$ that is allowed by the available hardware. Identification should be performed in closed-loop since the open-loop system (6) is unstable. Independent of the particular identification method used, the resulting nominal plant model $P_{d,h}$ should be FD LTI. Furthermore, a model of the plant with sampling frequency ω_s should be obtained, either by downsampling the model $P_{d,h}$ or by identifying the plant with sampling frequency ω_s. Finally, order reduction of both models can be performed.

Step 3: Quantify the performance goals by means of weighting filters. The purpose of the filters is twofold. Firstly, the static gain of the filters is used for scaling. Scaling is particularly useful for MIMO systems. Secondly, dynamical weighting filters are introduced to shape the resulting closed-loop TFM. Useful weighting filters for motion systems have been proposed in Steinbuch and Norg 1998 and in van de Wal *et al.* 2002. The weighting filters are parameterized by the target bandwidth of the control loop, by the frequency below which the controller should have integral action, and by the frequency beyond which the resulting controller should exhibit roll-off. This parametrization has a close relation with the familiar proportional-integral-derivative (PID) type controller. By applying the Tustin transformation to the plant model P_d, the weighting filters of Steinbuch and Norg 1998 and van de Wal *et al.* 2002 can be defined directly in the auxiliary w-domain.

Step 4: Quantify the model uncertainty (optional). There are always model uncertainties since no realistic system can be described exactly by a model. Such uncertainties are for instance introduced by changing operating conditions, neglected nonlinearities, higher order dynamics, or by the fact that data used for SI are obtained in a finite time interval and are contaminated

by noise. Let the uncertainty model be defined at the sampling frequency ω_s. The $\mathcal{H}_\infty$-norm is an induced norm that enables the explicit incorporation of model uncertainty in the control design procedure. A practically feasible procedure is presented in van de Wal *et al.* 2002. This procedure can be applied directly in the w-domain by means of the Tustin transformation.

Step 5: Compute the controller that minimizes the $\mathcal{H}_\infty$-norm of (45). If an uncertainty model is included, the resulting control problem is a robust performance problem and it makes sense to minimize the μ-seminorm instead of the $\mathcal{H}_\infty$-norm, see Skogestad and Postlethwaite 2005. Standard CT μ-synthesis tools, such as $D-K$-iterations, can be used if the problem is posed in the w-plane. Then, $K_d(w)$ is transformed back into the z-plane using (42) to enable implementation. This transformation does not involve any approximation, contrary to the commonly used discretization of CT (s-domain) controllers using the Tustin transformation (Chen and Francis 1995). Specifically, if $K_d(w)$ satisfies certain frequency domain specifications for $P_d(w)$ in terms of the fictitious frequency ν, then $K_d(z)$ satisfies the specifications for $P_d(z)$ for the true frequency ω.

5.2 *Addressing intersample behaviour*

The steps in § 5.1 enable the direct design of a DT controller using the setup of figure 4. However, the intersample behaviour issue has not been covered in the previous steps. In this section, the intersample behaviour issue is addressed using frequency domain MR tools. Given a DT controller K_d, which is operating at a sampling frequency ω_s, the resulting intersample response is determined by both the underlying plant dynamics $P_{d,h}$ and the exogenous inputs ω_h. Of course, the intersample response can easily be simulated for different exogenous inputs, but this is too time-consuming in general and does not give insight into the consequences of the digital controller implementation. Therefore, similar to the Bode diagram, the intersample response is analysed in the frequency domain. The main motivation is that the intersample response to exogenous inputs in a particular frequency band can easily be predicted, which resembles evaluating closed-loop transfer functions of LTI systems.

Step 6: Evaluate the control system including an intersample behaviour analysis. First of all, verify whether the controller that is computed in Step 5 satisfies the performance requirements for the system P_d, i.e., at the controller sampling instants. Then, verify whether the intersample response is satisfactory using the MR tools $\mathcal{F}$ and $\mathcal{P}$ of § 4. The frequency content of the exogenous signals should be known, where discrete frequencies are distinguished in the frequency band $[0, (\omega_{s,h}/2))$. If the intersample behaviour is not satisfactory, modify the weighting filters of Step 3 appropriately.

A remaining issue is how the weighting filters should be modified if the intersample behaviour is not satisfactory. Implementing a DT controller introduces a limitation on the achievable performance compared to a CT controller since the control signal u is restricted by ZOH interpolation. This implies that only disturbances below the Nyquist frequency $(\omega_s/2)$ can be attenuated effectively. More specifically, compared to CT control design, SD control design imposes an additional trade-off in the control design between the response to signals in the primary frequency band $|\omega| < (\omega_s/2)$ and the response to aliased signal components, i.e., signals in the frequency bands for which $|\omega| \geq (\omega_s/2)$.

The response to aliased signal components is determined by (26). The controller K_d only appears in Q_d, see (27). For the evaluation of the intersample behaviour in the frequency domain, it makes sense to evaluate the same transfer functions as in (45), yet unweighted and for the MR case, see figure 3. Regarding the closed-loop TFM M_d of (45), $G_{22,d}$ is equal to $-P_d$ and so

$$Q_d = -K_d S_d. \tag{47}$$

The response to aliased signal components is determined by the transfer function $K_d S_d$. The response of the MR system to aliased signal components is hence reduced by decreasing the magnitude of $K_d S_d$. The transfer function $K_d S_d$ can be changed by modification of the weighting filters in Step 2.

6. Application to a wafer stage

The design procedure of § 5 is applied to a wafer stage. The goal of this section is to illustrate (i) the design procedure of § 5, (ii) the purpose and use of the MR frequency domain intersample analysis tools, and (iii) the importance of intersample behaviour in practical applications. In § 6.1, the experimental setup is elaborated on. In § 6.2, the steps of § 5 are performed. Finally, in § 6.3 it is shown that improving the closed-loop performance at the controller sampling instants can deteriorate the intersample response.

6.1 *Experimental setup*

The experimental setup is a prototype wafer stage. The wafer stage is actuated and sensed in all six motion DOFs, see figure 6. Laser interferometers with sub-nanometer accuracy are used for sensing. By appropriate sensor and actuator transformations, the different

DOFs are rigid-body decoupled. The motion controllers are implemented in a discrete time state-space format. Though the design approach can handle the full MIMO control design problem (van de Wal *et al.* 2002), only the single-input single-output (SISO) control design in the z-direction is considered here to illustrate the intersample behaviour. The other directions are controlled by low-bandwidth PID controllers to avoid large interaction with other DOFs.

6.2 *Control design*

The six-step procedure of § 5 is performed. Throughout this section, the variable f is introduced to denote frequency, where $f_i = (\omega_i/2\pi)$ and i denotes an index, e.g., h or s.

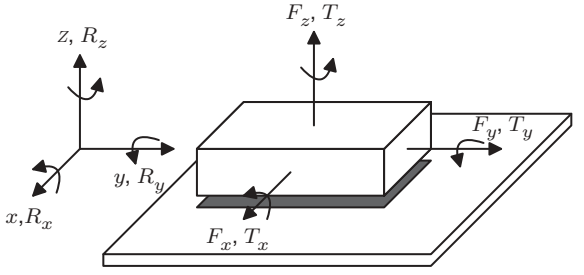

Figure 6. Schematic illustration of a wafer stage.

Step 1: The feedback control design of the system in figure 6 is considered in the z-direction. The interconnection structure of figure 5 is used, with corresponding TFM (45), where $n_u = n_y = 1$. The resulting controller is implemented with a sampling frequency $f_s = 1250$ Hz. However, it is possible to perform an identification experiment at $f_{s,h} = 5$ kHz, hence $F = 4$.

Step 2: Closed-loop SI has been performed to identify the plant. Since identification experiments are inexpensive, two identification experiments are performed at the sampling frequencies $f_s = 1250$ Hz and $f_{s,h} = 5$ kHz. An empirical transfer function estimate (ETFE) (Ljung 1999) is computed. Then the resulting frequency response data are approximated by a real-rational transfer function; see Pintelon and Schoukens 2001. The frequency points below 10 Hz are discarded due to a bad coherence. A balanced state-space realization is computed to enable the use of state-space optimization algorithms (Doyle *et al.* 1989) and to improve numerical conditioning. The plant model P_d that operates at a sampling frequency ω_s has a McMillan degree of 10, whereas the plant model $P_{d,h}$ that operates at the sampling frequency $f_{s,h}$ has McMillan degree 60. The latter model is only used for intersample behaviour analysis and its order does not influence the order of the resulting controller. Both identified models and frequency response functions are depicted in figure 7.

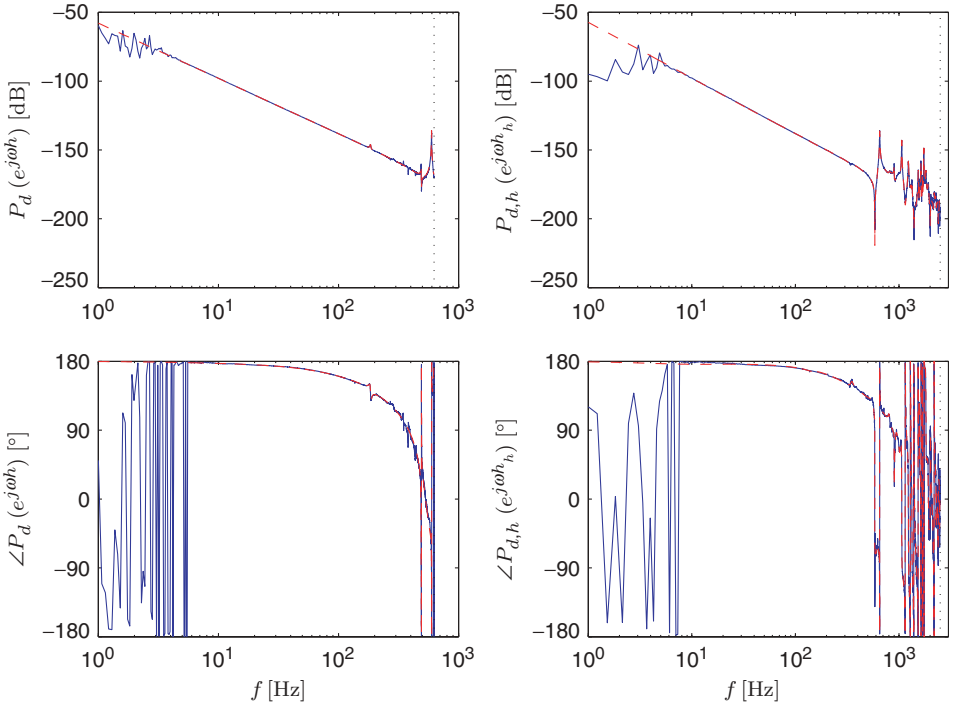

Figure 7. Identified frequency response functions (solid) and models (dashed). Left: sampling frequency $f_s = 1250$ Hz, right: sampling frequency $f_{s,h} = 5$ kHz.

Step 3: The performance goals are quantified by loopshaping-based weighting filters. These weighting filters are used to shape closed-loop transfer functions as suggested in van de Wal *et al.* 2002, Steinbuch and Norg 1998. The first step is to choose the target closed-loop bandwidth $f_{BW} \ll f_s$. In this experiment, $f_{\mathrm{BW}} = 60$ Hz. To facilitate the design procedure, the plant P_d is transformed into the auxiliary w-domain. The corresponding fictitious target bandwidth frequency ν_{BW}, resulting from substitution of $w = j\nu$ in (44), is given by $\nu_{BW} = (2/h)\tan(\pi f_{BW} h)$. Next, for scaling purposes, choose $V_{d,1} = 1$ and $V_{d,2} = |(P_d(w)|_{w=j\nu_{BW}})|^{-1}$. Hence, the resulting TFM is given by

$$M_d = -\begin{bmatrix} W_{d,1}S_d & W_{d,1}S_dP_d|(P_d(w)|_{w=j\nu_{BW}})|^{-1} \\ W_{d,2}K_dS_d & W_{d,2}K_dS_dP_d|(P_d(w)|_{w=j\nu_{BW}})|^{-1} \end{bmatrix}, \tag{48}$$

where $W_{d,1}$ is employed to enforce integral action up to a frequency $f_I < f_{BW}$ to achieve good low-frequent disturbance attenuation properties. In the w-domain, the corresponding frequency equals $\nu_I = (2/h)\tan(\pi f_I h)$. Below f_{BW} the frequency response of $P_d(w)$ approximately has a -2 slope, see (6). In the first row of M_d, see (48), the term $S_dP_d|(P_d(w)|_{w=j\nu_{BW}})|^{-1}$ in the second column is dominant over the first column at low frequencies. By defining

$$W_{d,1}(w) = \frac{w + \nu_I}{w}, \tag{49}$$

S_dP_d is enforced to have a $+1$ slope. If S_dP_d has a $+1$ slope and P_d a -2 slope, the controller necessarily has a -1 slope at low frequencies. Next, $W_{d,2}$ is defined such that the controller exhibits roll-off beyond a frequency f_R to reduce the amplification of measurement noise and to increase robustness against high-frequent model uncertainty. The static gain of $W_{d,2}$ is chosen such that the first and second row of M_d in (48) have approximately the same magnitude at ν_{BW}. Next, the plant rolls-off at high frequencies ($\nu \gg \nu_{BW}$) and $|S| \approx 1$. Then, K_dS_d dominates the $K_dS_dP_d|(P_d(w)|_{w=j\nu_{BW}})|^{-1}$ term in (48). By defining

$$W_{d,2}(w) = |(P_d(w)|_{w=j\nu_{BW}})|\alpha^2 \frac{w^2 + 2\beta_{R,1}\nu_R w + \nu_R^2}{w^2 + 2\beta_{R,2}\alpha\nu_R w + \alpha^2\nu_R^2}, \tag{50}$$

K_dS_d is enforced to roll-off with a slope -2, where $\nu_R = (2/h)\tan(\pi f_R h)$. Then, K_d also has a slope -2 at high frequencies ν since $S_d \to 1$ as $\nu \to \infty$. Furthermore, the damping ratios $\beta_{R,1}$ and $\beta_{R,2}$ are typically chosen equal to 0.7. The parameter α, typically chosen equal to 10, is introduced to ensure $W_{d,2}$ is proper and hence has a state-space realization. Furthermore, as a rule of thumb, $f_I < \frac{1}{4} f_{BW}$ and $f_R > 4 f_{BW}$, see van de Wal *et al.* 2002 for more details.

Step 4: No model uncertainty is considered.

Step 5: A suboptimal nominal controller $K_{d,nom}(w)$ is computed that satisfies the $\mathcal{H}_\infty$-norm bound

$$\|M_d(w)\|_\infty < \gamma, \tag{51}$$

where γ is minimized using a bisection algorithm (Doyle *et al.* 1989). The resulting controller $K_{d,nom}(w)$ is transformed into $K_{d,nom}(z)$ using (42), see also figure 8.

Step 6: The controller $K_{d,nom}$ resulting from $\mathcal{H}_\infty$-optimization is evaluated on the plant model P_d and the identified frequency response functions. From the closed-loop transfer functions, e.g., S_d in figure 8, it is concluded that $K_{d,nom}$ is a satisfactory nominal

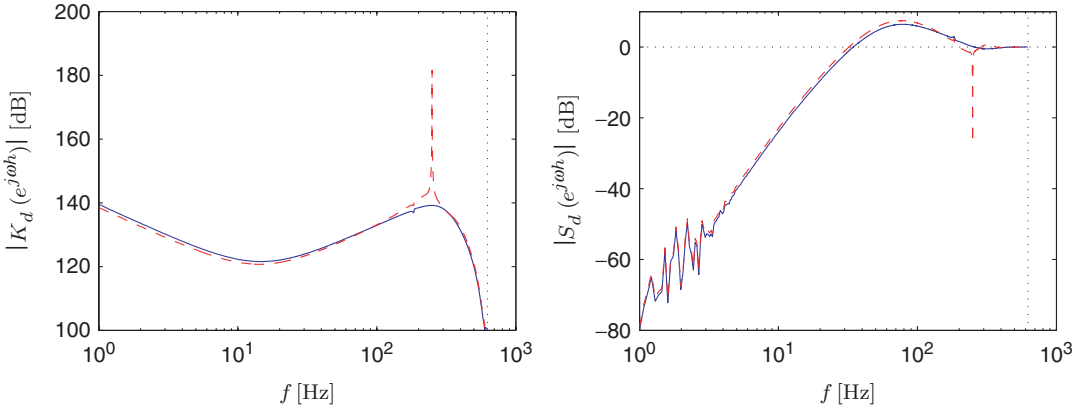

Figure 8. Left: controllers $K_{d,nom}$ (solid) and $K_{d,eb}$ (dashed). Right: DT sensitivity functions $S_{d,nom}$ (solid) and $S_{d,eb}$ (dashed) based on identified frequency response functions.

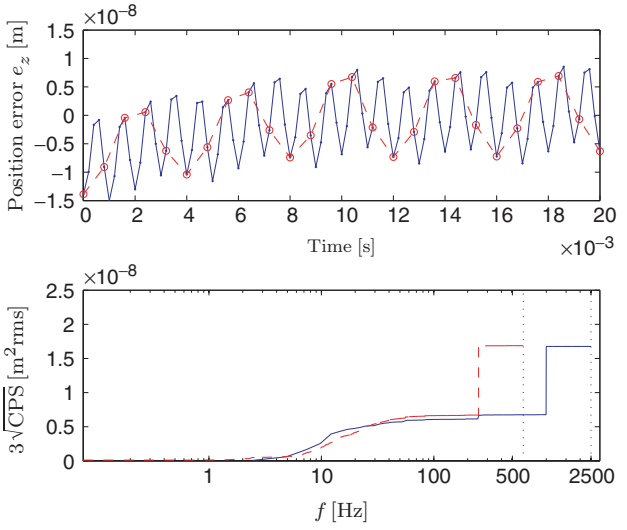

Figure 9. Measured error signals at $fs,h = 5$ kHz (solid) and at $f_s = 1250$ Hz (dashed) with $K_{d,nom}$ implemented.

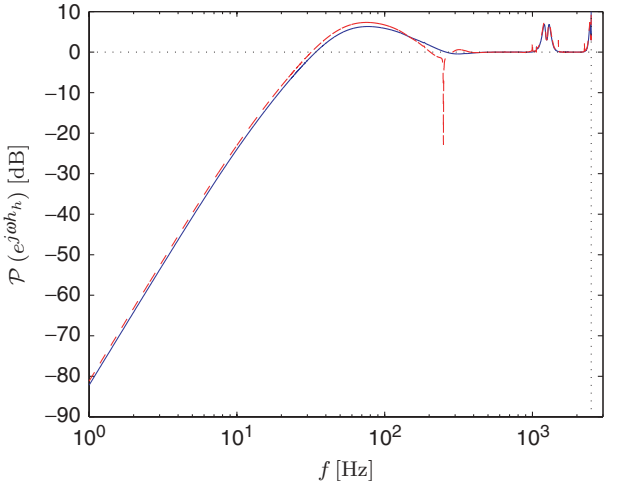

Figure 10. Multirate frequency domain analysis: $\mathcal{P}_{nom}$ (solid) and $\mathcal{P}_{eb}$ (dashed).

control design. Next, the controller is implemented on the experimental setup, where the reference ρ, see figure 2, is equal to zero. The resulting output is depicted in figure 9 at both the sampling frequencies f_s and $f_{s,h}$. Furthermore, both the time domain responses and cumulative power spectra (CPS) are depicted. It can be observed that the measurement with sampling frequency f_s contains a 250 Hz dominant component, whereas the measurement with sampling frequency $f_{s,h}$ contains a 1 kHz dominant component. Hence, it is concluded that aliasing occurs. The key question is whether the disturbance can effectively be attenuated by redesigning the controller. This is experimentally investigated in the next section, where the multirate analysis tools $\mathcal{F}$ and $\mathcal{P}$ are also employed.

6.3 *Error-based redesign*

An error-based redesign is made to account for the error spectrum measured at the controller sampling frequency f_s, i.e., intersample behaviour is neglected at this point in the design procedure. In particular, the weighting filters of Step 3 are modified using the approach suggested in van de Wal *et al.* 2000. The error-based controller redesign is denoted $K_{d,eb}$. A Bode magnitude plot of the controller is depicted in figure 8.

To evaluate disturbance attenuation properties the transfer function from ω_1 to ζ_1, see figure 5, is considered. This is motivated by the fact that the plant is assumed to be LTI, hence the disturbances can be associated with the plant output. The transfer functions corresponding to the nominal and error-based redesign are given by $S_{d,nom}$ and $S_{d,eb}$, respectively, see figure 8. Note that $S_{d,nom}$ and $S_{d,eb}$ are of the form (41) and thus give exact mappings between signals at controller sampling instants. $S_{d,eb}$ has a low gain compared to $S_{d,nom}$ at the discrete frequency of 250 Hz, which implies that the dominant disturbance will be attenuated effectively at the controller sampling instants. However, no conclusions can be drawn regarding the intersample response. To evaluate the intersample response, $\mathcal{P}$ is computed for both controllers K_d and $K_{d,eb}$, denoted $\mathcal{P}_{nom}$ and $\mathcal{P}_{eb}$, respectively, see figure 10.

Figure 10 shows that the magnitude of $\mathcal{P}_{eb}$ at 250 Hz is 28.4 dB lower than $\mathcal{P}_{nom}$. At 1 kHz, however, the magnitude of $\mathcal{P}_{eb}$ compared to $\mathcal{P}_{nom}$ is 2.85 dB higher. This implies that with the error-based redesign, the power of the intersample response reduces by 28.4 dB compared to the nominal design if the disturbance frequency is 250 Hz. However, the true disturbance is at 1 kHz, see figure 9. This implies that the power of the output increases by 2.85 dB compared to the nominal control design. This difference in gain illustrates the additional trade-off that arises in SD control design: below $(f_s/2)$ disturbances can be attenuated effectively, whereas (aliased) disturbances beyond $(f_s/2)$ result in deteriorated intersample behaviour.

The predictions of S_d and $\mathcal{P}$ are confirmed by experimental results, see figure 11. In particular, the disturbance is effectively attenuated at the controller sampling instants, as predicted by $S_{d,eb}$. The response in between the controller sampling instants is deteriorated compared to the nominal control design, as predicted by $\mathcal{P}_{nom}$ and $\mathcal{P}_{eb}$. No quantitative conclusions should be drawn from figure 9 and figure 11 since the measurement time is rather short.

The experimental results demonstrate the additional trade-off in SD control design between signals in the

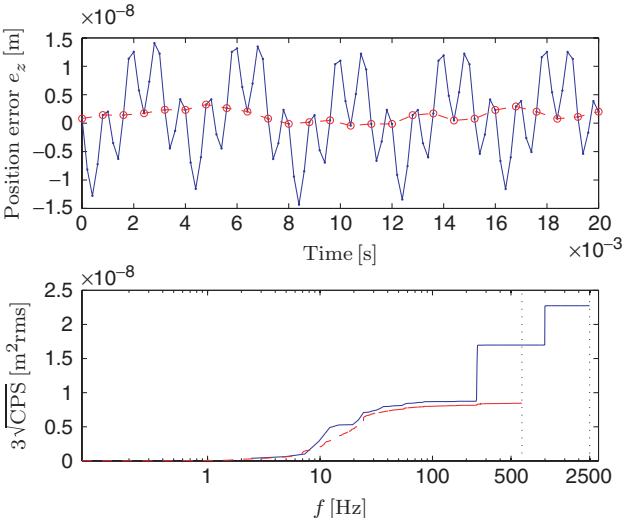

Figure 11. Measured error signals at $f_{s,h} = 5\,\text{kHz}$ (solid) and at $f_s = 1250\,\text{Hz}$ (dashed) with $K_{d,eb}$ implemented.

primary frequency band $\omega \in (-\omega_s/2, \omega_s/2)$ and aliased signals. $\mathcal{P}$ is a useful tool for predicting the power of the intersample response. To motivate that $\mathcal{R}$ is not suitable for performance analysis, write

$$\cos(j\omega) = \frac{1}{2}e^{j\omega} + \frac{1}{2}e^{-j\omega}, \tag{52}$$

i.e., real-valued sinusoidal signals of frequency ω can be written as the sum of two complex sinusoids with frequencies ω and $-\omega$. By writing the 250 Hz and 1000 Hz component as the sum of two complex sinusoids, it appears that their frequencies are in fact separated by f_s. Thus, $\mathcal{R}$ makes no distinction between input frequencies of 250 Hz and 1000 Hz. From $\mathcal{P}$, see figure 10, it is concluded that the 250 Hz disturbance can be effectively attenuated, while this is not the case for the 1000 Hz disturbance. Hence, $\mathcal{R}$ is not suitable for performance analysis.

7. Conclusions

An SD design framework covering the control design procedure from experimental modelling to digital controller implementation has been presented. Two problems that arise when both SI and direct optimal SD control design are incorporated into a control design cycle have been overcome. Firstly, the modelling problem has been resolved by replacing the SD synthesis problem with an MR synthesis problem. Secondly, the difficulties regarding the design aspect of LPTV systems have been overcome by separating the digital controller implementation from the intersample behaviour issue. The proposed design framework uses all intersample behaviour that can be obtained from experimental modelling. Furthermore, clear guidelines enable an iterative improvement of the intersample response to any desired extent. The proposed design framework has been applied to the feedback controller design of a wafer stage using $\mathcal{H}_\infty$ loopshaping. Although the presented framework has been applied to a specific system, its generality renders it applicable to other applications, SI techniques, and LTI controller synthesis approaches. The frequency domain analysis tools also provide insight into the cases where sampling zeros are cancelled, which is inherent to several control design approaches.

Open issues include the extension of the MR intersample behaviour analysis tools to a non-integer ratio of sampling frequencies, e.g., via sampling rate conversions. This extension would increase the generality of the proposed tools. Also, it is tacitly assumed that there is no sub-sample delay in the underlying CT system, e.g., due to computational delay. In the present approach, the delay is approximated by a real-rational transfer function and incorporated in the plant model. Explicitly incorporating the delay in the MR system as depicted in figure 3 may increase the accuracy of the plant model. Finally, the identification of the nominal model and uncertainty model in an MR setting require further research. In particular, a two step identification approach where the model is first identified at a high sampling frequency and subsequently downsampled to a lower sampling frequency may lead to more accurate models than direct identification at a low sampling frequency. The premise that a two step approach leads to more accurate models is motivated by the fact that more discrete frequencies are available for identification compared to the direct identification at a lower sampling frequency. Preliminary results in this direction can be found in Oomen *et al.* (2007). Additionally, it is worthwhile to investigating the effects of downsampling to the size and structure of the uncertainty model.

References

B.D.O. Anderson, "Controller design: moving from theory to practice", *Cont. Syst. Mag.*, 13, pp. 16–25, 1993.

M. Araki, Y. Ito and T. Hagiwara, "Frequency response of sampled-data systems", *Automatica*, 32, pp. 483–497, 1996.

K.J. Åström and B. Wittenmark, *Computed-Controlled Systems: Theory and Design*, 2nd ed., Engle-wood Cliffs, NJ: Prentice-Hall, 1990.

K.J. Åström, P. Hagander and J. Sternby, "Zeros of sampled systems", *Automatica*, 20, pp. 31–38, 1984.

G.J. Balas, J.C. Doyle, K. Glover, A. Packard and R. Smith, *μ-Analysis and Synthesis Toolbox*, 3rd ed., Natick, MA: μ-Analysis and Synthesis Toolbox, 2001.

B. Bamieh, "Intersample and finite wordlength effects in sampled-data problems", *IEEE Trans. Autom. Cont.*, 48, pp. 639–643, 2003.

B. Bamieh and J.B. Pearson, "The $\mathcal{H}_2$ problem for sampled-data systems", *Syst. Cont. Lett.*, 19, pp. 1–12, 1992a.

B.A. Bamieh and J.B. Pearson, "A general framework for linear periodic systems with applications to $\mathcal{H}_\infty$ sampled-data control", *IEEE Trans. Autom. Cont.*, 37, pp. 418–435, 1992b.

B. Bamieh, M.A. Dahleh and J.B. Pearson, "Minimization of the $\mathcal{L}_\infty$-induced norm for sampled-data systems", *IEEE Trans. Autom. Cont.*, 38, pp. 717–732, 1993.

B. Bamieh, J.B. Pearson, B.A. Francis and A. Tannenbaum, "A lifting technique for linear periodic systems with applications to sampled-data control", *Syst. Cont. Lett.*, 17, pp. 79–88, 1991.

H.W. Bode, *Network Analysis and Feedback Amplifier Design*, London, UK: Van Nostrand, 1945.

J.W. Brown and R.V. Churchill, *Complex Variables and Applications*, 6th ed., New York, NY: McGraw-Hill, 1996.

M.W. Cantoni and K. Glover, "Frequency-domain analysis of linear periodic operators with application to sampled-data control design", in *Conference on Decision and Control*, San Diego, CA, 1997, pp. 4318–4323.

M. Cantoni and G. Vinnicombe, "Controller discretization: a gap metric framework for analysis and synthesis", *IEEE Trans. Autom. Cont.*, 49, pp. 2033–2039, 2004.

T. Chen and B. Francis, *Optimal Sampled-Data Control Systems*, London, UK: Springer, 1995.

J.C. Doyle and G. Stein, "Multivariable feedback design: concepts for a classical/modern synthesis", *IEEE Trans. Autom. Cont.*, 26, pp. 4–16, 1981.

J.C. Doyle, K. Glover, P.P. Khargonekar and B.A. Francis, "State-space solutions to standard $\mathcal{H}_2$ and $\mathcal{H}_\infty$ control problems", *IEEE Trans. Autom. Cont.*, 34, pp. 831–947, 1989.

M.J. Englehart and M.C. Smith, "A four-block problem for $\mathcal{H}_\infty$ design: properties and applications", *Automatica*, 27, pp. 811–818, 1991.

G.F. Franklin, J.D. Powell and M. Workman, *Digital Control of Dynamic Systems*, 3rd ed., Menlo Park, CA: Addison Wesley Longman, 1998.

J.S. Freudenberg, R.H. Middleton and J.H. Braslavsky, "Inherent design limitations for linear sampled-data feedback systems", *Int. J. Cont.*, 61, pp. 1387–1421, 1995.

G.C. Goodwin and M. Salgado, "Frequency domain sensitivity functions for continuous time systems under sampled data control", *Automatica*, 30, pp. 1263–1270, 1994.

M. Hirata, T. Atsumi and K. Nonami, "High performance digital servo design for HDD by using sampled-data $\mathcal{H}_\infty$ control design", in *International Workshop on Advanced Motion Control*, Nagoya, Japan, 2000, pp. 86–91.

P.A. Iglesias and K. Glover, "State-space approach to discrete-time $\mathcal{H}_\infty$ control", *Int. J. Cont.*, 54, pp. 1031–1073, 1991.

R.E. Kalman, Y.C. Ho and K. Narendra, Controllability of linear dynamical systems, in *Controllability of Linear Dynamical Systems*, New York, NY: Interscience, 1963, 189–213.

J.P. Keller and B.D.O. Anderson, "A new approach to the discretization of continuous-time controllers", *IEEE Trans. Autom. Cont.*, 37, pp. 214–223, 1992.

T. Kimura, H. Fujioka, K. Tokai and T. Takamori, "Sampled-data $\mathcal{H}_\infty$ control for a pneumatic cylinder system", in *Conference on Decision and Control*, Kobe, Japan, 1996, pp. 759–760.

G.M. Kranc, "Input-output analysis of multirate feedback systems", *IRE Trans. Autom. Cont.*, 3, pp. 21–28, 1957.

O. Lindgärde and B. Lennartson, "Performance and robust frequency response for multirate sampled-data systems", in *American Control Conference*, Albuquerque, NM, 1997, pp. 3877–3881.

L. Ljung, *System Identification: Theory for the User*, 2nd ed., Upper Saddle River, NJ: Prentice Hall, 1999.

C.A. Mack, "The new, new limits of optical lithography", in *Proceedings of the Emerging Lithographic Technologies*, 5374, Santa Clara, CA, 2004, pp. 1–8.

D. McFarlane and K. Glover, "A loop shaping design procedure using $\mathcal{H}_\infty$ synthesis", *IEEE Trans. Autom. Cont.*, 37, pp. 759–769, 1992.

T. Oomen, M. van de Wal and O. Bosgra, "Exploiting $\mathcal{H}_\infty$ sampled-data control theory for high-precision electromechanical servo control design", in *American Control Conference*, Minneapolis, MN, 2006, pp. 1086–1091.

T. Oomen, M. van de Wal and O. Bosgra, "Aliasing of resonance phenomena in sampled-data control design: hazards, modelling, and a solution", in *American Control Conference*, New York, NY, accepted, 2007.

R. Pintelon and J. Schoukens, *System Identification: A Frequency Domain Approach*, New York, NY: IEEE Press, 2001.

H. Sandberg and B. Bernhardsson, "A Bode sensitivity integral for linear time-periodic systems", *IEEE Trans. Autom. Cont.*, 50, pp. 2034–2039, 2005.

S. Skogestad and I. Postlethwaite, *Multivariable Feedback Control: Analysis and Design*, 2nd ed., West Sussex, , England: John Wiley & Sons, 2005.

M. Steinbuch and M.L. Norg, "Advanced motion control: an industrial perspective", *Eur. J. Cont.*, 4, pp. 278–293, 1998.

G. Stix, "Toward 'point one'", *Scientific American*, 272, pp. 72–77, 1995.

H.K. Sung and S. Hara, "Properties of sensitivity and complementary sensitivity functions in single-input single-output digital control systems", *Int. J. Cont.*, 48, pp. 2429–2439, 1988.

P.P. Vaidyanathan, *Multirate Systems and Filter Banks*, Engle-wood Cliffs, NJ: Prentice Hall, 1993.

M. van de Wal, G. van Baars and F. Sperling, "Reduction of residual vibrations by $\mathcal{H}_\infty$ feedback control", in *Motion and Vibration Conference*, Sydney, Australia, 2000, pp. 481–487.

M. van de Wal, G. van Baars, F. Sperling and O. Bosgra, "Multivariable $\mathcal{H}_\infty/\mu$ feedback control design for high-precision wafer stage motion", *Cont. Eng. Pract.*, 10, pp. 739–755, 2002.

P.M.R. Wortelboer, "Frequency-weighted balanced reduction of closed-loop mechanical servo systems: theory and tools". PhD thesis, Delft University of Technology, Delft, The Netherlands (1993).

Y. Yamamoto and P.P. Khargonekar, "Frequency response of sampled-data systems", *IEEE Trans. Autom. Cont.*, 41, pp. 166–176, 1996.

Y. Yamamoto, A.G. Madievski and B.D.O. Anderson, "Approximation of frequency response for sampled-data control systems", *Automatica*, 35, pp. 729–734, 1999.

K. Zhou, J.C. Doyle and K. Glover, *Robust and Optimal Control*, Upper Saddle River, NJ: Prentice Hall, 1996.